[American Journal of Science, Vol. 316, April, 2016, P. 309–328, DOI 10.2475/04.2016.01]

American Journal of Science

APRIL 2016

INTERLAYER GROWTH KINETICS OF A BINARY SOLID-SOLUTION BASED ON THE THERMODYNAMIC EXTREMAL PRINCIPLE: APPLICATION TO THE FORMATION OF SPINEL AT PERICLASE-CORUNDUM CONTACTS

RAINER ABART*,†, JIRI SVOBODA**, PETR JEŘABEK***, ERWIN POVODEN-KARADENIZ§, and GERLINDE HABLER*

ABSTRACT. A thermodynamic model has been developed for interlayer growth in a binary system between two phases of fixed composition producing an intermediate solid-solution phase. Thereby long-range diffusion, interface migration and generation/annihilation of vacancies at the reaction interfaces have been considered as potentially rate limiting. The coupling among these processes governs overall growth rate, position of the Kirkendall plane and the compositions of the solid-solution phase at the reaction interfaces. Model calculations illustrating the relations between the corresponding kinetic parameters and system evolution are presented. In particular, the systematics of non-equilibrium element partitioning across moving reaction interfaces is addressed. It is found that the deviation from equilibrium element partitioning at a moving reaction interface is a more sensitive monitor for the departure from local equilibrium than the deviation from parabolic growth behavior. Finally, the model is applied to interlayer growth of magnesio-aluminate spinel.

Keywords: reactive dffusion, interface migration, thermodynamic modeling, spinel

INTRODUCTION

Growth of a new phase forming a layer along the contacts between two mutually incompatible reactant phases is a common phenomenon in solid-state reactions. In mineralogical sciences the corresponding phenomenon is referred to as reaction rim or corona formation (Vernon, 2004). Interlayer growth is also encountered in technical applications such as in the engineering of composite materials, coatings, welding, corrosion, and in thin-film electronic devices.

Generally, the reactant and product phases have different compositions, and interlayer growth requires long-range diffusion of chemical components across the growing layer and localized reactions at the reaction interfaces on either side of the layer. The overall process is referred to as reactive diffusion (Svoboda and Fischer, 2013). It has been shown theoretically and in experiment that interlayer growth is parabolic, if local equilibrium is maintained at the reaction interfaces (Koch and Wagner, 1936; Schmalzried, 1981; Schneider and Inden, 2004; Svoboda and others, 2006). In this case system evolution is exclusively controlled by long-range diffusion. This has motivated a series of rim growth experiments in binary systems such as MgO –

* University of Vienna, Department of Lithospheric Research, Althanstrasse 14, A-1090 Vienna, Austria
** Institute of Physics of Materials, Academy of Sciences of the Czech Republic, Zizkova 22, CZ-61662 Brno, Czech Republic
*** Institute of Petrology and Structural Geology, Faculty of Science, Charles University in Prague, Albertov 6, CZ-12843 Prague, Czech Republic
§ Institute of Materials Science and Technology, Christian Doppler Laboratory for Early Precipitation, Vienna University of Technology
† Corresponding author: rainer.abart@univie.ac.at

SiO_2 (Brady, 1983; Fisler and others, 1997; Yund, 1997; Milke and others, 2001; Gardes and others, 2011), $CaCO_3$ – SiO_2 (Milke and Heinrich, 2002), MgO – Al_2O_3 (Carter, 1961; Rossi and Fulrath, 1963; Watson and Price, 2002; Götze and others, 2010; Keller and others, 2010), and in metal systems (van Dal and others, 2000a; van Dal and others, 2000b) aiming to determine effective diffusion coefficients from measured layer-growth rates.

Local equilibrium at reaction interfaces requires perfectly mobile reaction interfaces implying instantaneous interface reactions. In general, interface reactions do, however, proceed at finite rates, and, as a consequence, reaction interfaces have finite mobilities. If interface reactions become rate limiting, interlayer growth is linear (Dybkov, 1986; Balluffi and others, 2005). Depending on the relative efficiencies of long-range diffusion and interface reactions interlayer growth may thus show different kinetic behavior. It tends to be interface reaction controlled during early growth stages, when transport distances are short, and diffusion is effective. Interlayer growth becomes successively more prone to diffusion control, when layer thickness increases during later growth stages (Dybkov, 1986; Abart and Petrishcheva, 2011). Linear growth (Cserhati and others, 2008) and linear growth followed by a gradual transition to parabolic growth (Götze and others, 2014) was indeed observed experimentally for very thin, on the order of 100 nm thick, layers. For μm thick layers obtained from thick diffusion couples parabolic growth was generally observed (Navias, 1961; Whitney and Stubican, 1971; Zhang and others, 1996; Watson and Price, 2002; Liu and others, 2005; Götze and others, 2010).

Moreover, finite interface mobilities imply chemical potential jumps and, as a consequence, deviations from equilibrium element partitioning across a moving reaction interface (Gamsjäger, 2007). Models accounting for simultaneous long range diffusion and reaction interfaces with finite mobility have been presented by several authors (Deal and Grove, 1965; Schmalzried, 1974; Farrell and others, 1975; Gösele, and Tu, 1982; Dybkov, 1986; Abart and Petrishcheva, 2011; Svoboda and Fischer, 2013). These studies did, however, not address composition variation in the newly formed intermediate phase (Abart and Petrishcheva, 2011; Svoboda and Fischer, 2013) or did not properly account for the Kirkendall effect (Dybkov, 1986).

The Kirkendall effect has repeatedly been documented experimentally in reactive diffusion (van Dal and others, 2000a; van Dal and others, 2000b; Abart and others, 2004, 2009; Gardes and others, 2011). This implies that vacancies are generated and/or annihilated at reaction interfaces. Depending on their microscopic structure reaction interfaces may serve as more or less efficient sources and sinks for vacancies. The ease of vacancy generation/annihilation at reaction interfaces influences overall reaction kinetics and generation/annihilation of vacancies at reaction interfaces must be considered as a potentially rate limiting process (Svoboda and Fischer, 2013).

In general, interlayer growth follows mixed kinetics governed by the coupling among long-range diffusion, interface migration, and generation/annihilation of vacancies at the reaction interfaces. In this communication we present a thermodynamic model for reactive diffusion in a binary system with two reactant phases of fixed composition and an intermediate solid-solution phase with a limited solubility range. We allow for long-range diffusion, interface migration and generation/annihilation of vacancies at reaction interfaces as potentially rate limiting processes. From a kinematic analysis a set of relations among the kinetic variables with four degrees of freedom is obtained. The thermodynamic extremal principle (Ziegler, 1961; Svoboda and Turek, 1991; Svoboda and others, 2005; Martyushev and Seleznev, 2006; Fischer and others, 2014) is then employed to solve for the kinetic variables. The influence of the kinetic parameters on system evolution is investigated using a hypothetical example. Finally

the model is applied to growth of mangesio-aluminate spinel ($MgAl_2O_4$) at the contact between periclase (MgO) and corundum (Al_2O_3).

THERMODYNAMIC MODEL

The Thermodynamic Extremal Principle

In the following a model for interlayer growth of a solid-solution phase in a binary system is derived based on the thermodynamic extremal principle (Svoboda and Turek, 1991). Growth is assumed to occur close to equilibrium, so that linear kinetics can be applied (De Groot and Mazur, 1984), and the generalized thermodynamic fluxes J_i are related to the generalized thermodynamic forces F_k as (Callen, 1985)

$$J_i = \sum_k L_{ik} F_k \tag{1}$$

where L_{ik} is a matrix of kinetic coefficients. The rate of entropy production Q associated with the fluxes in a non-equilibrium system reads (Callen, 1985)

$$Q_j = \sum_k F_k J_k \tag{2}$$

Based on maximization of the entropy production rate (dissipation) Onsager (1931) showed that for heat flux in anisotropic media

$$L_{ik} = L_{ki}, \tag{3}$$

and a more general variational approach to this extremal principle was given by Ziegler (1961). Through the formulation of the thermodynamic extremal principle (TEP) in terms of the characteristic system parameters Svoboda and Turek (1991) provided a versatile tool for modeling irreversible processes in complex systems. According to the TEP the independent thermodynamic fluxes attain the values that maximize the rate of entropy production at any time. In a closed system, the rate of entropy production is equal to the negative rate of free energy change $\dot{G}$, so that the system is governed by

$$\max\ Q + \lambda(Q + \dot{G}), \tag{4}$$

where λ is a Lagrange multiplier. After some algebra this yields the system of linear equations (Svoboda and Turek, 1991)

$$-\frac{1}{2}\sum_i \frac{\partial^2 Q}{\partial J_i \partial J_i} J_i = \frac{\partial \dot{G}}{\partial J_i} \tag{5}$$

Solving equations (5) for the fluxes provides a numerical scheme for describing system evolution in terms of successive time-steps. In the following the TEP is adopted for solving the specific problem of interlayer growth, where linear kinetics is assumed for all processes involved.

Problem Posing

Let us assume a binary system with components A and B containing two phases of fixed composition α (pure A) and β (pure B) and an intermediate solid-solution phase γ with composition $A_{1-r}B_r$, where r is the mole fraction of component B (fig. 1A). The

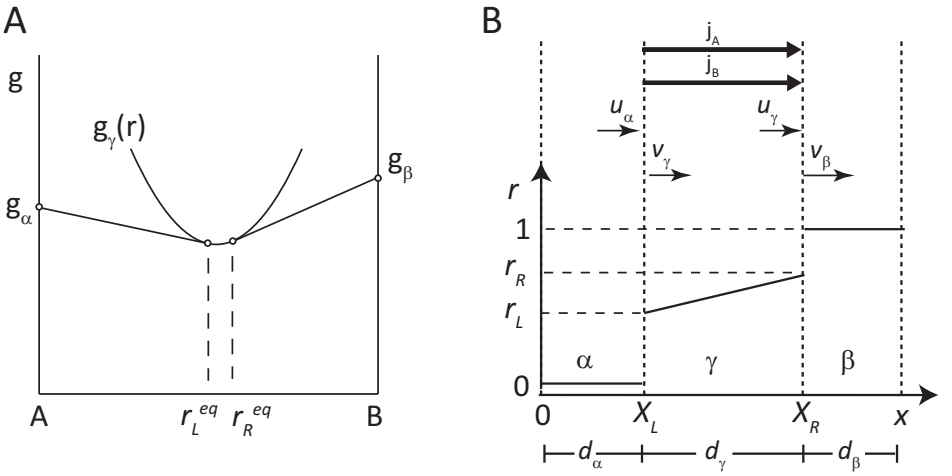

Fig. 1. (A) Schematic molar Gibbs energy diagram for fixed pressure and temperature of the binary system A – B with phases α and β of fixed composition and molar Gibbs energies g_α and g_β and a solid-solution phase γ with Gibbs energy $g_\gamma(r)$, where r is the mole fraction of component B; r_L^{eq}, and r_R^{eq} are the compositions of the solution phase γ at the left (contact with α) and right (contact with β) interface. (B) System geometry and phase compositions during layer growth, X_L and X_R are the positions of the left and right interface, r_L and r_R are the compositions of γ at the left and right interfaces, they do, in general, not correspond to equilibrium compositions and evolve with time, d_α, d_β, and d_γ are the width of the respective phase domains; small arrows indicate interface velocities u and v relative to the lattices of the phases on either side of the interface (subscripts), thick arrows indicate component fluxes.

molar Gibbs energies of the α and β phases are denoted by g_α and g_β. The composition-dependent molar Gibbs energy of phase γ is approximated[1] by

$$g_r(r) = W_2 r^2 + W_2 r + W_0. \tag{6}$$

As a starting configuration we choose an assembly of phase γ to the left and phase β to the right in contact at a planar interface with inert markers. The coordinate normal to the interface is denoted x, and t is time. We assume that during a negligible time a very thin layer of phase γ forms at the original α – β interface and starts to grow as schematically depicted in figure 1B. To keep the following derivations simple and based on empirical findings (see below) the composition profile in phase γ is taken as linear in x with

$$r = r_L + \frac{(r_R - r_L)(x - X_L)}{X_R - X_L}, \tag{7}$$

where r_L and r_R are the compositions of γ at the left and right reaction interface with positions X_L and X_R, respectively. The reaction interfaces have finite mobilities M_L and M_R, and are considered as non-ideal sources and sinks for vacancies, where the ease of vacancy generation/annihilation is described by the activities of vacancy generation/annihilation U_L and U_R. The diffusion fluxes j_A and j_B of the components A and B are restricted to the domain occupied by phase γ and are zero in both reactant phases. The interface mobilities, the activities of vacancy generation/annihilation, and the respec-

[1] A more rigorous formulation would involve the term $R_g T\,(r \ln r + (1-r)\ln(1-r))$ with R_g being the gas constant and T the absolute temperature, which accounts for configurational entropy. We only consider a small solubility range of γ delimited by r_L and r_R with $(r_R - r_L) << 1$. In this case the configurational entropy term is nearly a constant, which is accounted for by W_0 in equation (6).

tive diffusion coefficients are considered as phenomenological constants. The molar volumes of the phases α, β, and γ are denoted Ω_α, Ω_β, and Ω_γ. The velocities u_α and v_β refer to motion of the left interface relative to the lattices of phases α and β, respectively. Similarly, the velocities u_γ and v_β refer to motion of the right interface relative to the lattices of phases γ and β, respectively.

Kinematics

Conservation of mass across the moving interfaces requires

$$\frac{u_\alpha}{\Omega_\alpha} - \frac{v_y(1 - r_L)}{\Omega_\gamma} = -j_{A_L}, \tag{8}$$

$$\frac{v_\gamma r_L}{\Omega_\gamma} = j_{B_L}, \tag{9}$$

$$\frac{u_\gamma(1 - r_R)}{\Omega_\gamma} = j_{A_R}, \tag{10}$$

$$\frac{u_\gamma r_R}{\Omega_\gamma} - \frac{v_\beta}{\Omega_\beta} = j_{B_R}. \tag{11}$$

From mass balance in the bulk of phase γ we obtain

$$j_{A_L} - j_{A_R} = -\int_{X_L}^{X_R} \frac{\dot{r}}{\Omega_\gamma} dx, \tag{12}$$

$$j_{B_L} - j_{B_R} = -\int_{X_L}^{X_R} \frac{\dot{r}}{\Omega_\gamma} dx. \tag{13}$$

For use in later derivations the interface velocities are defined with respect to two different reference systems: If the coordinate system is fixed to the left end of the specimen we have

$$\frac{\partial X_L}{\partial t} = u_\alpha, \tag{14}$$

$$\frac{\partial X_R}{\partial t} = u_\alpha - v_\gamma + u_\gamma. \tag{15}$$

Alternatively, if the coordinate system is fixed to the lattice of phase γ, the time derivatives of the interface positions read

$$\dot{X}_L = v_\gamma, \tag{16}$$

and

$$\dot{X}_R = u_\gamma. \tag{17}$$

The system evolution is described by 14 kinetic variables $\frac{\partial X_L}{\partial t}$, $\frac{\partial X_B}{\partial t}$, $\dot{X}_L$, $\dot{X}_R$, $\dot{r}_L$, $\dot{r}_R$, j_{A_L}, j_{A_R}, j_{B_L}, j_{B_R}, u_α, v_γ, u_γ, v_β constrained by ten equations, eqs. (8–17). The system has four degrees of freedom. The rates $\frac{\partial X_L}{\partial t}$, $\frac{\partial X_B}{\partial t}$, $\dot{r}_L$, $\dot{r}_R$ would be the most convenient for

describing the system as they refer to directly measurable quantities. However, the remaining kinetic parameters cannot be eliminated easily, and an alternative set of kinetic variables $\dot{r}_L$, $\dot{r}_R$, u_α, v_γ, u_γ, v_β constrained by two additional relations (see equations 27 and 28) is used.

Total Gibbs Energy

The total Gibbs energy G can be written as

$$G = \frac{g_\alpha d_\alpha}{\Omega_\alpha} + \frac{g_\beta d_\beta}{\Omega_\beta} + \int_{X_L}^{X_R} \frac{g_\gamma}{\Omega_\gamma}\, dx, \tag{18}$$

where g_γ is given by eq. (6). For differentiation of G with respect to time we use $\dot{d}_\alpha = u_\alpha$, $\dot{d}_\beta = -v_\beta$ and with the coordinate system fixed to the lattice of phase γ we obtain

$$\dot{G} = \frac{g_\alpha}{\Omega_\alpha} u_\alpha - \frac{g_\beta}{\Omega_\beta} v_\beta + \frac{1}{\Omega_\beta}\left[- v_\gamma g_\gamma(r_L) + u_\gamma g_\gamma(r_R) + \int_{X_L}^{X_R} \frac{dg_\gamma}{dr}\dot{r}\, dx \right], \tag{19}$$

where the expression in square brackets accounts for the free energy change due to growth of γ at the interfaces first and second term) and due to continuous composition change (integral expression) and

$$\dot{r} = \left(1 - \frac{x - X_L}{X_R - X_L}\right)\dot{r}_L + \frac{x - X_L}{X_R - X_L}\dot{r} + \left[\frac{(r_R - r_L)(x - X_L)}{(X_R - X_L)^2} - \frac{r_R - r_L}{X_R - X_L}\right] v_\gamma - \frac{(r_R - r_L)(x - X_L)}{(X_R - X_L)^2} u_\gamma. \tag{20}$$

Inserting eq. (20) into eq. (19) and performing the integral the partial derivatives of G with respect to the kinetic variables $\frac{\partial \dot{G}}{\partial \dot{r}_L}$, $\frac{\partial \dot{G}}{\partial \dot{r}_R}$, $\frac{\partial \dot{G}}{\partial u_\alpha}$, $\frac{\partial \dot{G}}{\partial v_\gamma}$, $\frac{\partial \dot{G}}{\partial u_\gamma}$, $\frac{\partial \dot{G}}{\partial v_\beta}$ are obtained. The explicit expressions are provided in the electronic supplementary material (http://earth.geology.yale.edu/%7eajs/SupplementaryData/2016/02Abart.pdf).

Total Gibbs Energy Dissipation

Gibbs energy is assumed to dissipate by diffusion in the bulk of phase γ, by migration of the reaction interfaces, and by generation/annihilation of vacancies at the reaction interfaces.

The relative velocity of the $\alpha - \gamma$ interface with respect to the lattices of the adjacent phases is approximated by the average $(u_\alpha + v_\beta)/2$, and similarly at the $\gamma - \beta$ interface by the average $(u_\gamma + v_\beta)/2$. The rate of deposition of atoms (thickening rate) at the $\alpha - \gamma$ interface is given by the difference $(v_\gamma + u_\alpha)$ and similarly at the $\gamma - \beta$ interface by the difference $(v_\beta + u_\gamma)$.

For the independent diffusive flux j_i of a component i driven by the gradient in its chemical potential $\nabla\mu_i$ we have $j_i = L_{ii}\nabla\mu_i$ and the associated dissipation reads $Q = j_i\nabla\mu_i = \frac{j_i^2}{L_{ii}}$ (see equation 2). Noting that $L_{ii} = \frac{D_i}{R_g T}$, where R_g is the gas constant, T is absolute temperature, and D_i is the effective tracer diffusion coefficient of component i, the dissipation due to diffusion in the bulk of phase γ is

$$Q_d = R_g T \Omega_\gamma \int_{X_L}^{X_R} \frac{j_A^2}{(1-r)D_A} + \frac{j_B^2}{rD_B} dx, \tag{21}$$

where D_A and D_B are the tracer diffusion coefficients of components A and B in phase γ, or the effective tracer diffusion coefficients, if γ is a polycrestal. Using eqs. (8) and (12) the flux of component A is expressed as

$$J_A(x) = \frac{u_\alpha}{\Omega_\alpha} + \frac{\nu_\gamma}{\Omega_\gamma}(1 - r_L) + \int_{X_L}^{x} \frac{\dot{r}}{\Omega_\gamma} dx, \tag{22}$$

similarly using eqs. (9) and (13) the flux of component B is

$$J_B(x) = \frac{\nu_\gamma}{\Omega_\gamma} r_L - \int_{X_L}^{x} \frac{\dot{r}}{\Omega_\gamma} dx. \tag{23}$$

Inserting from eqs. (22) and (23) into eq. (21) an explicit expression for the dissipation due to diffusion is obtained. Following the logic leading to equation (21), the dissipation due to migration of the interfaces reads

$$Q_m = \frac{(u_\alpha + \nu_\gamma)^2}{4M_L} + \frac{(u_\gamma + \nu_\beta)^2}{4M_R}, \tag{24}$$

and the dissipation due to generation/annihilation of vacancies at the interfaces is given by

$$Q_{a/g} = \frac{(\nu_\gamma - u_\alpha)^2}{U_L} + \frac{(\nu_\beta - u_\gamma)}{U_R}. \tag{25}$$

The total dissipation is then

$$Q = Q_d + Q_m + Q_{a/g}. \tag{26}$$

Performing the first and second derivatives with respect to the kinetic variables yields expressions of the form

$$\frac{\partial^2 Q}{\partial \xi_i \, \partial \xi_j}, \qquad i,j = 1,\ldots 6,$$

where $\boldsymbol{\xi}_i$ and $\boldsymbol{\xi}_j$ are the kinetic variables $\dot{r}_L$, $\dot{r}_R$, u_α, ν_γ, u_γ. The explicit expressions are provided in the electronic supplementary material (http://earth.geology.yale.edu/%7eajs/SupplementaryData/2016/02Abart.pdf).

Kinetic Equations

Inserting eqs. (8–11) and (20) into constraints (12) and (13) and performing the integral additional constraints can be written as

$$\bar{\alpha}_1 \dot{r}_L + \bar{\beta}_1 \dot{r}_R + \bar{\gamma}_1 u_\alpha + \bar{\delta}_1 \nu_\gamma + \overline{\in}_1 u_\gamma + \bar{\varnothing}_1 \nu_\beta = 0, \tag{27}$$

$$\bar{\alpha}_2 \dot{r}_L + \bar{\beta}_2 \dot{r}_R + \bar{\gamma}_2 u_\alpha + \bar{\delta}_2 \nu_\gamma + \overline{\in}_2 u_\gamma + \bar{\varnothing}_2 \nu_\beta = 0, \tag{28}$$

with

$$\begin{aligned}
\bar{\alpha}_1 = \bar{\beta}_1 &= \frac{x_R - x_L}{2\Omega_\gamma}, & \bar{\alpha}_2 &= \bar{\beta}_2 = \frac{x_L - x_R}{2\Omega_\gamma},\\
\bar{\gamma}_1 &= -\frac{1}{\Omega_\alpha}, & \bar{\gamma}_2 &= 0,\\
\bar{\delta}_1 &= -\overline{\in}_1 = \frac{2 - r_L - r_R}{2\Omega_\gamma}, & \bar{\delta}_2 &= -\overline{\in}_2 = \frac{r_L + r_R}{2\Omega_\gamma},\\
\bar{\varnothing}_1 &= 0, & \bar{\varnothing}_2 &= \frac{1}{\Omega_\beta}.
\end{aligned} \tag{29}$$

The kinetic variables $\dot{r}_L$, $\dot{r}_R$, u_α, ν_γ, u_γ, and ν_β constrained by eqs. (27) and (28) are now determined by application of the thermodynamic extremal principle (Svoboda and Turek, 1991), which for the case at hand yields the system of equations

$$\begin{aligned}
&\frac{1}{2}\frac{\partial^2 Q}{\partial \dot{r}_L^2}\dot{r}_L + \frac{1}{2}\frac{\partial^2 Q}{\partial \dot{r}_L \partial \dot{r}_R}\dot{r}_R + \frac{1}{2}\frac{\partial^2 Q}{\partial \dot{r}_L \partial u_\alpha}u_\alpha + \frac{1}{2}\frac{\partial^2 Q}{\partial \dot{r}_L \partial \nu_\gamma}\nu_\gamma +\\
&\frac{1}{2}\frac{\partial^2 Q}{\partial \dot{r}_L \partial u_\gamma}u_\gamma + \frac{1}{2}\frac{\partial^2 Q}{\partial \dot{r}_L \partial \nu_\beta}\nu_\beta + \bar{\alpha}_1\lambda_1 + \bar{\alpha}_2\lambda_2 = -\frac{\partial \dot{G}}{\partial \dot{r}_L},\\
&\frac{1}{2}\frac{\partial^2 Q}{\partial \dot{r}_L \partial \dot{r}_R}\dot{r}_L + \frac{1}{2}\frac{\partial^2 Q}{\partial \dot{r}_R^2}\dot{r}_R + \frac{1}{2}\frac{\partial^2 Q}{\partial \dot{r}_R \partial u_\alpha}u_\alpha + \frac{1}{2}\frac{\partial^2 Q}{\partial \dot{r}_R \partial \nu_\gamma}\nu_\gamma +\\
&\frac{1}{2}\frac{\partial^2 Q}{\partial \dot{r}_R \partial u_\gamma}u_\gamma + \frac{1}{2}\frac{\partial^2 Q}{\partial \dot{r}_R \partial \nu_\beta}\nu_\beta + \bar{\beta}_1\lambda_1 + \bar{\beta}_2\lambda_2 = -\frac{\partial \dot{G}}{\partial \dot{r}_R},\\
&\frac{1}{2}\frac{\partial^2 Q}{\partial \dot{r}_L \partial u_\alpha}\dot{r}_L + \frac{1}{2}\frac{\partial^2 Q}{\partial \dot{r}_R \partial u_\alpha}\dot{r}_R + \frac{1}{2}\frac{\partial^2 Q}{\partial u_\alpha^2}u_\alpha + \frac{1}{2}\frac{\partial^2 Q}{\partial u_\alpha \partial \nu_\gamma}\nu_\gamma +\\
&\frac{1}{2}\frac{\partial^2 Q}{\partial u_\alpha \partial u_\gamma}u_\gamma + \frac{1}{2}\frac{\partial^2 Q}{\partial u_\alpha \partial \nu_\beta}\nu_\beta + \bar{\gamma}_1\lambda_1 + \bar{\gamma}_2\lambda_2 = -\frac{\partial \dot{G}}{\partial u_\alpha},\\
&\frac{1}{2}\frac{\partial^2 Q}{\partial \dot{r}_L \partial \nu_\gamma}\dot{r}_L + \frac{1}{2}\frac{\partial^2 Q}{\partial \dot{r}_R \partial \nu_\gamma}\dot{r}_R + \frac{1}{2}\frac{\partial^2 Q}{\partial u_\alpha \partial \nu_\gamma}u_\alpha + \frac{1}{2}\frac{\partial^2 Q}{\partial \nu_\gamma^2}\nu_\gamma +\\
&\frac{1}{2}\frac{\partial^2 Q}{\partial \nu_\gamma \partial u_\gamma}u_\gamma + \frac{1}{2}\frac{\partial^2 Q}{\partial \nu_\gamma \partial \nu_\beta}\nu_\beta + \bar{\delta}_1\lambda_1 + \bar{\delta}_2\lambda_2 = -\frac{\partial \dot{G}}{\partial \nu_\gamma},\\
&\frac{1}{2}\frac{\partial^2 Q}{\partial \dot{r}_L \partial u_\gamma}\dot{r}_L + \frac{1}{2}\frac{\partial^2 Q}{\partial \dot{r}_R u_\gamma}\dot{r}_R + \frac{1}{2}\frac{\partial^2 Q}{\partial u_\alpha \partial u_\gamma}u_\alpha + \frac{1}{2}\frac{\partial^2 Q}{\partial \nu_\gamma \partial u_\gamma}\nu_\gamma +\\
&\frac{1}{2}\frac{\partial^2 Q}{\partial u_\gamma^2}u_\gamma + \frac{1}{2}\frac{\partial^2 Q}{\partial u_\gamma \partial \nu_\beta}\nu_\beta + \overline{\in}_1\lambda_1 + \overline{\in}_2\lambda_2 = -\frac{\partial \dot{G}}{\partial u_\gamma},\\
&\frac{1}{2}\frac{\partial^2 Q}{\partial \dot{r}_L \partial \nu_\beta}\dot{r}_L + \frac{1}{2}\frac{\partial^2 Q}{\partial \dot{r}_R \partial \nu_\beta}\dot{r}_R + \frac{1}{2}\frac{\partial^2 Q}{\partial u_\alpha \partial \nu_\beta}u_\alpha + \frac{1}{2}\frac{\partial^2 Q}{\partial \nu_\gamma \partial \nu_\beta}\nu_\gamma +\\
&\frac{1}{2}\frac{\partial^2 Q}{\partial u_\gamma \partial \nu_\beta}u_\gamma + \frac{1}{2}\frac{\partial^2 Q}{\partial \nu_\beta^2}\nu_\beta + \bar{\phi}_1\lambda_1 + \bar{\phi}_2\lambda_2 = -\frac{\partial \dot{G}}{\partial \nu_\beta}
\end{aligned} \tag{30}$$

where λ_1 and λ_2 are Lagrange undetermined multipliers. Starting from a specific initial configuration and integrating the solutions of the system of eqs. (27), (28), and (30) over successive time steps provides a numerical scheme for simulating system evolution for a given set of kinetic parameters.

Model Calculations

The results of model calculations illustrating the influence of the kinetic parameters on system evolution are shown in figure 2. Calculations were done for a hypotheti-

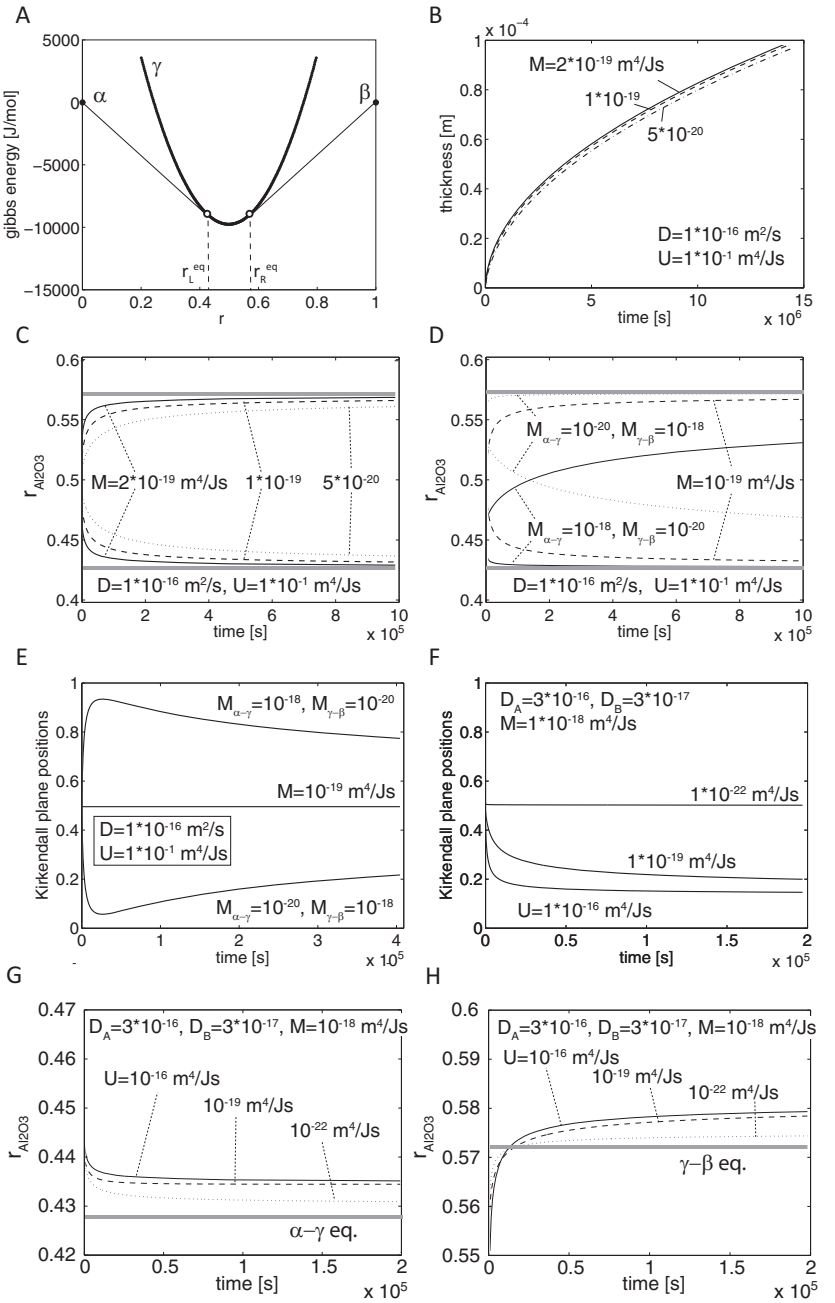

Fig. 2. (A) Molar Gibbs energy diagram of hypothetical model system. (B) Thickness of γ – phase layer as a function of time for three interface mobilities. (C and D) Composition evolution of γ phase at the α – γ interface (lower curves) and at the γ – β interface (upper curves) for three interface mobilities, $r_{Al_2O_3}$ is the mole fraction of Al_2O_3, horizontal gray bars indicate equilibrium compositions of phase γ at the α – γ (lower bar) and the γ – β (upper bar) interface. (E) Position of the Kirkendall plane relative to the positions of the two reaction interfaces, which are at positions 0 and 1, respectively, for a given diffusivity ratio and for different interface mobilities. (F) Relative position of Kirkendall plane for given diffusivity ratio and different activities for vacancies at reaction interfaces. (G and H) influence of the activity for generation/annihilation of vacancies on the compositions of phase γ at the α – γ and the γ – β interface; horizontal gray bars indicate equilibrium compositions of phase γ at the respective reaction interface - see text for further explanation.

cal system, where the Gibbs energies were chosen as $g_\alpha = g_\beta = 0$ J/mol and $g_\gamma = W_2 (r - 0.5)^2 + W_0$ with $W_2 = 15 \times 10^4$ J/mol and $W_0 = -1 \times 10^4$J/mol (fig. 2A). The molar volumes were taken as $\Omega_\alpha = \Omega_\beta = \Omega_\gamma = 10^{-5}$ m^3/mole. In figures 2B and C the influence of interface mobility is shown for a fixed choice of tracer diffusion coefficients, $D_A = D_B = 10^{-16}$ m^2/s and activities for generation/annihilation of vacancies at the interfaces, $U_{\alpha-\gamma} = U_{\gamma-\beta} = 10^{-1}$m^4/Js. Three different interface mobilities, $M_{\alpha-\gamma} = M_{\gamma-\beta} = 1 \times 10^{-19}$m^4/Js, 5×10^{-20}m^4/Js, and 2.5×10^{-20}m^4/Js were chosen. The equilibrium compositions of phase γ at the α–γ and at the γ–β interfaces are given by the common tangent construction to the g_γ - curve yielding $r_L^{eq} = 0.43$ and $r_R^{eq} = 0.57$ (fig. 2A). They are indicated for reference by gray bars in figures 2C, D, G, and H. For all model calculations the initial thickness of the γ - layer was taken as 5×10^{-7}m.

Despite of finite interface mobilities nearly parabolic growth is obtained (fig. 2B). Lowering interface mobility leads to slower growth, but for the range of interface mobilities chosen, only a minute deviation from parabolic growth results. In figure 2C the evolution of interface compositions is shown for the same range of interface mobilities as in figure 2B. Note that initially the compositions of phase γ at the reaction interfaces deviate substantially from the corresponding equilibrium compositions being displaced towards more intermediate compositions. They gradually approach equilibrium compositions as interlayer growth proceeds. The rate at which equilibrium compositions are approached decreases with decreasing interface mobility. While the deviation from parabolic growth is rather subtle (fig. 2B), the deviation from equilibrium compositions of phase γ at the reaction interfaces is rather pronounced. The composition of a solid solution phase at a moving reaction interface appears to be a more sensitive monitor for departure from local equilibrium than the growth behavior.

The effect of different interface mobilities for fixed tracer diffusivities and activities for vacancy generation/annihilation at the reaction interfaces is illustrated in figure 2D. The dashed lines show the evolution of the interface compositions for $M_{\alpha-\gamma} = M_{\gamma-\beta} = 1 \times 10^{-19}$m^4/Js (compare fig. 2C), the dotted lines correspond to $M_{\alpha-\gamma} = 10^{-20}$m^4/Js, $M_{\gamma-\beta} = 1 \times 10^{-18}$m^4/Js, and the solid lines represent the scenario with $M_{\alpha-\gamma} = 10^{-18}$m^4/Js, $M_{\gamma-\beta} = 1 \times 10^{-20}$m^4/Js. The interface composition of phase γ is "repelled" from the equilibrium composition at the interface with lower mobility. This is due to the fact that jumps in chemical potential at a reaction interface increase with decreasing interface mobility. Given that the reactant phase has fixed composition, an increase in chemical potential jump implies that the composition of the intermediate solid-solution phase is shifted further from the equilibrium composition. Moreover, the equilibrium composition is approached more rapidly at the interface with high mobility than at the interface with low mobility.

If growth were only diffusion controlled (perfectly mobile reaction interfaces acting as ideal sources and sinks for vacancies), the relative diffusivities of the A and B components would exclusively determine the relative fluxes of the A and B components and, as a consequence, the position of the Kirkendall plane (Svoboda and others, 2006; Abart and others, 2009). If reaction interfaces with finite mobility and acting as non ideal sources/sinks for vacancies are involved, the position of the Kirkendall plane does not only depend on relative component diffusivities but is also influenced by the interface mobilities and by the activities for generation/annihilation of vacancies at the reaction interfaces. In figure 2E the positions of the Kirkendall planes for the scenarios presented in figure 2D are shown. The positions of the Kirkendall planes are shown relative to the positions of the $\alpha - \gamma$ and the $\gamma - \beta$ interfaces, which were taken as 0 and 1, respectively. Even if the tracer diffusivities are similar for both components, the Kirkendall plane is at different positions within the γ layer for different interface mobilities. The Kirkendall plane is in a central position, if

both interface mobilities are similar. If the two interfaces have different mobilities, the Kirkendall plane is closer to the interface with lower mobility. The offset of the Kirkendall plane relative to the position it would have for purely diffusion controlled layer growth is most pronounced during early growth stages. The Kirkendall plane successively approaches the position for diffusion controlled growth with increasing layer thickness.

The Kirkendall effect implies generation and/or annihilation of vacancies at the reaction interface. In figure 2F the position of the Kirkendall plane within the γ – layer is shown for the case that $D_B/D_A = 0.1$ and for fixedinterface mobilities $M_{\alpha-\gamma} = M_{\gamma-\beta} = 1 \times 10^{-18}\mathrm{m}^4/\mathrm{Js}$. Three values were applied for the activity for generation/annihilation of vacancies at the interfaces $U_{\alpha-\gamma} = U_{\gamma-\beta} = 1 \times 10^{-16}\mathrm{m}^4/\mathrm{Js}$, $1 \times 10^{-19}\mathrm{m}^4/\mathrm{Js}$ and $1 \times 10^{-22}\mathrm{m}^4/\mathrm{Js}$. The lower the activity for generation/annihilation of vacancies at the interfaces, the stronger the difference in the interface velocities with respect to the lattices of the two adjacent phases and thus the Kirkendall effect is suppressed. Low values of U force the replacement at the respective interface to occur at close to constant volume. This provides an additional constraint and influences the overall kinetics. If the activity of generation/annihilation of vacancies at the reaction interfaces is low, the Kirkendall plane is at a central position despite of different tracer diffusivities of the A and B components. If layer growth were only diffusion controlled, the Kirkendall plane would be predicted at a relative position of 0.09 for $D_B/D_A = 0.1$. This position is approached at late growth stages at different rates, depending on the value of U.

In figures 2G and 2H the compositions of phase γ at the reaction interfaces is shown for the same diffusivity ratio as applied in figure 2F for scenarios with different activities for generation/annihilation of vacancies. For the hypothetical system at hand, vacancies need to be generated/annihilated only, when the diffusivities of the two components differ. In figures 2G and 2H the component diffusivities were chosen as $D_A = 3 \times 10^{-16}\mathrm{m}^2/\mathrm{s}$, $D_B = 3 \times 10^{-17}\mathrm{m}^2/\mathrm{s}$ so that $D_B/D_A = 0.1$. The interface mobilities were taken as $M_{\alpha-\gamma} = M_{\gamma-\beta} = 1 \times 10^{-18}\mathrm{m}^4/\mathrm{Js}$, and three values of U were chosen, $U_{\alpha-\gamma} = U_{\gamma-\beta} = 1 \times 10^{-16}\mathrm{m}^4/\mathrm{Js}$, $10^{-19}\mathrm{m}^4/\mathrm{Js}$, and $10^{-22}\mathrm{m}^4/\mathrm{Js}$. It is seen in figures 2G and 2H that at both reaction interfaces the compositions of phase γ are displaced from the equilibrium compositions towards higher concentrations of the component with lower diffusivity. For a given diffusivity ratio, the effect is most pronounced at high activities for generation/annihilation of vacancies, and it is suppressed, if the activities for generation/annihilation of vacancies are low. For the case at hand phase γ grows with a non-equilibrium composition outside the solubility limits at the γ − β interface, that is at the interface towards the source of the less mobile component, and with a non-equilibrium composition within the solubility limit at the α − γ interface. This effect is suppressed, if the activity for generation/annihilation of vacancies is low. Growth of a supersaturated phase γ bears potential for secondary relaxation phenomena such as precipitation of phase β in the bulk of phase γ.

In summary, employing the thermodynamic extremal principle for modeling the coupling among long-range diffusion, interface motion and generation/annihilation of vacancies at interfaces during layer growth yields a wide range of phenomena regarding growth behavior, element partitioning at moving reaction interfaces, and with respect to the position of the Kirkendall pane. In particular, under the simplifying assumption of a linear composition variation across the growing layer of the solid-solution phase it predicts a systematic evolution of the compositions of the solid-solution phase at the reaction interfaces starting with substantial deviations from equilibrium partitioning and a gradual approach of equilibrium element partitioning as interlayer growth proceeds.

In the next section, this model is applied to layer growth in the MgO – Al_2O_3 system, where a systematic evolution of spinel compositions at the interfaces to reactant periclase and corundum has indeed been documented.

APPLICATION TO SPINEL INTERLAYER GROWTH

Interlayer growth of magnesio-aluminate spinel ($MgAl_2O_4$) at contacts between periclase (MgO) and corundum (Al_2O_3) occurs by interdiffusion of Al^{3+} versus Mg^{2+} while oxygen largely remains in place (Carter, 1961; Rossi and Fulrath, 1963). Generally parabolic growth was observed experimentally and thermodynamic analyses based on the assumption of local equilibrium at the reaction interfaces were performed for determining component diffusivities (Schmalzried, 1962; Pfeiffer and Schmalzried, 1989; Watson and Price, 2002; Götze and others, 2010).

More recently linear growth followed by an evolution towards parabolic growth was observed for ≤100 nm thick spinel layers forming at the contacts between single crystal corundum and a thin MgO coating (Götze and others, 2014). Such growth behavior indicates a transition from interface-reaction control to mixed kinetics and implies departure from local equilibrium at one or both of the reaction interfaces. Due to the small thickness of the spinel layer element partitioning across the reaction interfaces, which could potentially be employed for quantifying deviations from local equilibrium, could not be determined. Jeřabek and others (2014) investigated microstructure and texture evolution in magnesio-aluminate spinel grown at the contacts between single crystal periclase and corundum under uniaxial load. Similar to earlier studies (Watson and Price, 2002; Götze and others, 2010) they observed a linear composition variation across the growing spinel layer with spinel being relatively more Mg-rich towards the spinel-periclase interface and relatively more Al-rich towards the spinel-corundum interface. In addition, Jeřabek and others (2014) documented nonequilibrium element partitioning at the reaction interfaces. In particular, a systematic evolution of the element partitioning, which is incompatible with growth at constant pressure and temperature conditions of the experiment, was observed at the spinel-corundum interface. In the following we investigate the evolution of spinel compositions as obtained from time series experiments by Jeřabek and others (2014)

Experimental

Layer growth experiments were done using oriented synthetic single crystals of periclase and corundum, which were in contact at a polished interface. Run conditions were 1350 °C and ambient pressure. In addition, uniaxial load of 29 MPa was applied to ensure good mechanical contact between the two crystals. Run durations were 5 to 160 h. Details of the experimental procedure, microstructure and composition analysis are given in the electronic supplementary material (http://earth.geology.yale.edu/%7eajs/SupplementaryData/2016/02Abart.pdf). The evolution of spinel compositions expressed in terms of $r_{Al_2O_3} = \frac{Al_2O_3}{Al_2O_3 + MgO}$ in molar proportions is shown in figure 3. Spinel is relatively magnesium-rich at the interface with periclase and shows a linear increase in aluminium content towards the interface with corundum. It is important to note that the Mg/Al partitioning across the reaction interfaces is substantially displaced from equilibrium initially and evolves towards local equilibrium partitioning at later growth stages (fig. 3D).

Thermodynamic Analysis

Equilibrium phase relations in the MgO – Al_2O_3 system have been investigated repeatedly (Sack, 1982, 2014; Sack and Ghiorso, 1991; Hallstedt, 1992; Jung and others, 2004). In this context, the disordering of spinel, represented by the degree of

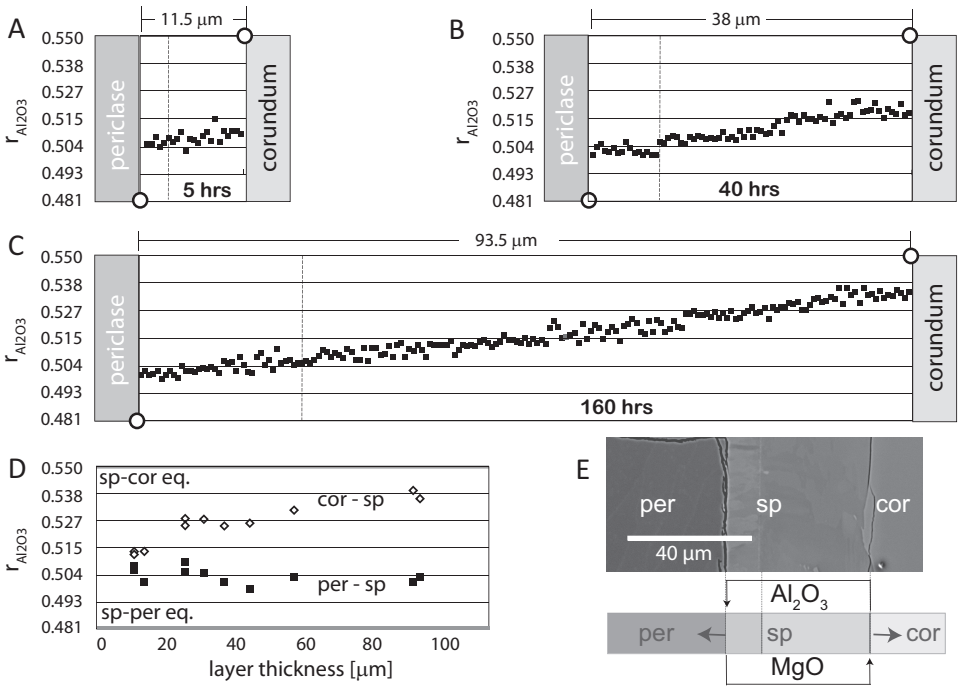

Fig. 3. Composition variation of spinel for annealing times of (A) 5 hours, (B) 40 Hours, (C) 160 hours. Vertical dashed lines show position of the Kirkendall plane; note that with increasing layer thickness (annealing time) an approximately linear composition trend from relatively Al − rich spinel at the spinel-corundum interface towards more Mg – rich spinel at the spinel-periclase interface develops. The equilibrium compositions of spinel $r^{sp(per)}_{Al_2O_3} \approx 0.48$, $r^{sp(cor)}_{Al_2O_3} \approx 0.55$ at the reaction interfaces are indicated by open circles. (D) Evolution of spinel compositions at the reaction interfaces, horizontal gray bars indicate equilibrium compositions of spinel at the reaction interfaces; note that the equilibrium compositions are approached at different rates at the two reaction interfaces and are not fully attained after 160 hours corresponding to 90 μm rim thickness; (E) BSE image and schematic illustration of experimental setting.

inversion, is a critical property. Whereas Jung and others (2004) did not report on their treatment of spinel disordering, the thermodynamic assessment of Hallstedt (1992) exactly reproduced the experimentally determined inversion of Wood and others (1986), which are erroneously high (see fig. 10 in Hallstedt 1992). Later experiments consistently revealed substantially lower degrees of inversion (Gobbi and others, 1985; Millard and others, 1992; Andreozzi and others, 2000; Pavese and others, 2000; Andreozzi and Princivalle, 2002; Sack, 2014). In a recent computational thermodynamic assessment of the system (Zienert and Fabrichnaya, 2013) spinel inversion was re-modeled, resulting in close agreement with these experiments. Moreover, Zienert and Fabrichnaya (2013) obtained excellent agreement with experimental equilibrium phase boundaries, including both solubilities of MgO and Al_2O_3 in spinel. This is why the thermodynamic data from Zienert and Fabrichnaya (2013) are used in the following treatment.

For application of equations (30) the Gibbs energy of spinel as obtained from the assessment of Zienert and Fabrichnaya (2013) is approximated by a polynomial in $r_{Al_2O_3}$, which is obtained from equilibrium phase relations calculated using Thermocalc Version S based on the thermodynamic data of Zienert and Fabrichnaya (2013) (see table 1. To satisfy the constraints imposed by the calculated phase relations a third order polynomial of the form $g_{sp} = W_3 r^3 + W_2 r^2 + W_1 r + W_0$ was used, where the parameters W_0 through W_3 were obtained from solving the system of equations

Table 1

Gibbs energies

	per	cor	sp(per)	sp(cor)
g [J/mol]	-711666.0	-1911104.5	-1302251.6	-1390440.8
$r_{Al_2O_3}$	0	1	0.47965	0.55385
Ω [cm^3/mol]	11.85	26.51	20.63	20.63

Equilibrium compositions of spinel at spinel-periclase and spinel-corundum contacts, and molar volumes of the phases normalized to one mole of components: periclase (MgO), corundum (Al_2O_3), and spinel ($Mg_{0.5}AlO_2$) as obtained using Thermocalc Version S based on a recent reassessment of thermodynamic data (Zienert and Fabrichnaya, 2013).

$$\begin{aligned}
\frac{g_{per} - g_{sp}(r_{Al_2O_3}^{sp(per)})}{r_{Al_2O_3}^{sp(per)}} &= 3W_3(r_{Al_2O_3}^{sp(per)})^2 + 2W_2(r_{Al_2O_3}^{sp(per)}) + W_1 \\
\frac{g_{sp}(r_{Al_2O_3}^{sp(cor)}) - g_{cor}}{1 - r_{Al_2O_3}^{sp(cor)}} &= 3W_3(r_{Al_2O_3}^{sp(cor)})^2 + 2W_2(r_{Al_2O_3}^{sp(cor)}) + W_1 \\
g_{sp}(r_{Al_2O_3}^{sp(per)}) &= W_3(r_{Al_2O_3}^{sp(per)})^3 + W_2(r_{Al_2O_3}^{sp(per)})^2 + W_1(r_{Al_2O_3}^{sp(per)}) + W_0 \\
g_{sp}(r_{Al_2O_3}^{sp(cor)}) &= W_3(r_{Al_2O_3}^{sp(cor)})^3 + W_2(r_{Al_2O_3}^{sp(cor)})^2 + W_1(r_{Al_2O_3}^{sp(cor)}) + W_0.
\end{aligned} \tag{31}$$

Inserting the values for $r_{Al_2O_3}^{sp(per)}$, $r_{Al_2O_3}^{sp(cor)}$, $g_{sp}(r_{Al_2O_3}^{sp(per)})$, $g_{sp}(r_{Al_2O_3}^{sp(per)})$, g_{per}, and g_{cor} from table 1 yields $W_0 = 265400$ J/mol, $W_1 = -1415900$ J/mol, $W_2 = 2310600$ J/mol, $W_3 = -1206200$ J/mol. A comparison between spinel Gibbs energy obtained from Thermocalc Version S based on the thermodynamic data of Zienert and Fabrichnaya (2013) with the polynomial approximation is shown in the electronic supplementary material (http://earth.geology.yale.edu/%7eajs/SupplementaryData/2016/02Abart.pdf).

The system of equations (30) completed by constraints (27) and (28) was then used for calculating system evolution while systematically varying the kinetic parameters D_{MgO}, $D_{Al_2O_3}$, M_{per-sp}, M_{cor-sp}, U_{per-sp}, and U_{cor-sp}. From fitting the model to the combined experimental data including layer thickness as a function of time, evolution of element partitioning at the reaction interfaces, and the position of the Kirkendall plane within the spinel layer the kinetic parameters were determined as $M_{per-sp} = 7.7 \times 10^{-16}$[m^4/Js], $M_{cor-sp} = 7.2 \times 10^{-15}$[m^4/Js], $M_{per-sp}/M_{cor-sp} \approx 0.1$, $D_{MgO} = 2.9 \times 10^{-15}$, $D_{Al_2O_3} = 9.3 \times 10^{-15}$, $D_{Al_2O_3} = D_{MgO} \approx 3$ and $U_{per-sp} = U_{cor-sp} \geq 10^{-11}$ (see table 2). A comparison between experimental observations and model calculations is shown in figure 4. Good agreement between experimental data and modeling results is obtained for all features, including rim growth rate (fig. 4A), evolution of element

Table 2

Kinetic parameters obtained from fitting model calculations to the experimental results

D_{MgO} [m^2/s]	$D_{Al_2O_3}$ [m^2/s]	M_{per-sp} [m^4/Js]	M_{cor-sp} [m^4/Js]	U_{per-sp} [m^4/Js]	U_{cor-sp} [m^4/Js]
2.9 x 10^{-15}	9.3 x 10^{-15}	7.7 x 10^{-16}	7.2 x 10^{-15}	$\geq 10^{-11}$	$\geq 10^{-11}$

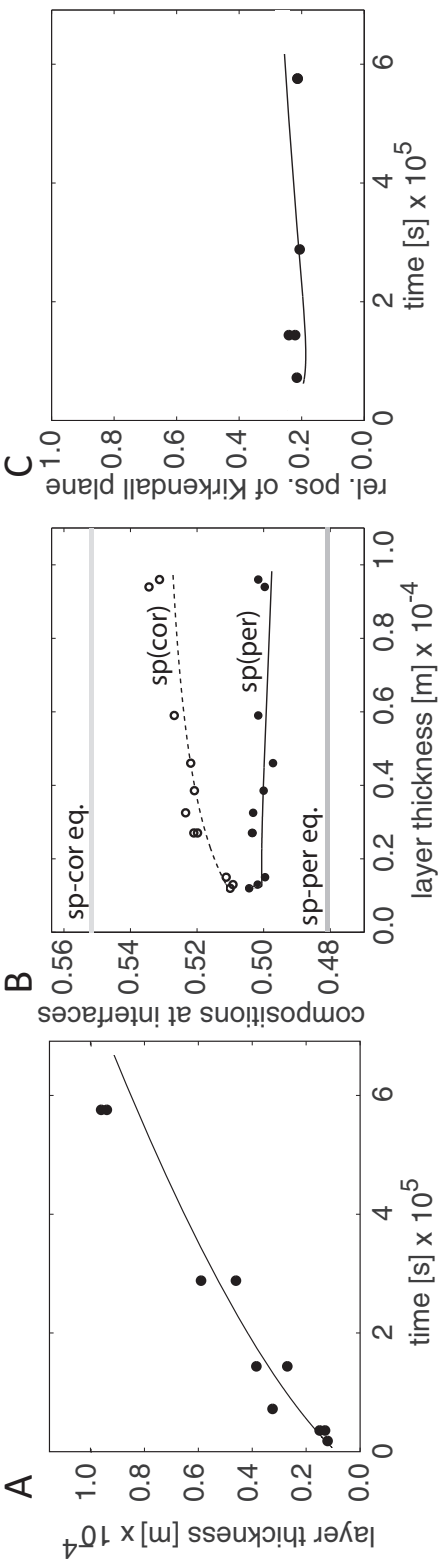

Fig. 4. (A) Layer thickness as a function of time, black circles-experimental data, solid line-model fit. (B) Composition of spinel at the reaction interfaces as a function of layer thickness; open and closed circles represent experimental data for spinel compositions at the spinel-corundum and at the spinel-periclase interface, respectively, dashed and solid curves are the corresponding model fits using the kinetic parameters given in table 2; horizontal gray bars show equilibrium compositions of spinel at the two reaction interfaces. (C) Relative position of the Kirkendall plane; black circles-experimental data based ontextural change (observed only in five run product), solid line-model fit.

partitioning at the reaction interfaces (fig. 4B), and position of the Kirkendall plane within the spinel layer (fig. 4C).

Qualitatively the relative interface mobilities with $M_{per-sp}/M_{cor-sp} \approx 0.1$ can be inferred from the fact that the equilibrium composition of spinel is approached at a slower rate at the spinel-periclase interface than at the spinel corundum interface. The relatively low mobility of the periclase-spinel interface is probably due to its semi-coherent nature (Jeřabek and others, 2014). Using atomic- resolution scanning transmission electron microscopy Li and others (submitted[2]) found pinning of the spinel-periclase interface due to the slow climb of misfit edge dislocations, which occur at the interface at about every 23'rd (100) and (010) spinel lattice plane. In addition pores, which are typically present at this interface, but are absent at the spinel-corundum interface (see electronic supplementary material for further discussion; http://earth.geology.yale.edu/%7eajs/SupplementaryData/2016/02Abart.pdf) are dragged along by the periclase-spinel interface further contributing to its finite mobility. The finding that $M_{per-sp} < M_{cor-sp}$ is in conflict with the supposition of Götze and others (2014), who suggested that $M_{per-sp} > M_{cor-sp}$ for spinel layer growth in thin films. The experiments of Götze and others (2014) were made at 900 and 1000 °C, some 350 to 450 °C below the temperatures of the experiments of Jeřabek and others (2014), and the experimental results can only be compared with caution. Nevertheless, it may be hypothesised that the apparent discrepancy is due to the fact that the two studies monitor different stages of rim growth. Whereas, Götze and others (2014) investigated growth of spinel layers less than about 100 nm thick, the range of layer thicknesses analysed in this study is from about ten to 100 μm. It is well possible that the atomic structures and thus the mobilities of the reaction interfaces are different during incipient and advanced stages of layer growth (Hesse and others, 1994; Sieber and others, 1997a, 1997b). The incipient stages of layer growth can, however, not be assessed with the experiments Jeřabek and others (2014), and the kinetics of incipient layer growth cannot be constrained.

The relative diffusivities with $D_{Al_2O_3}/D_{MgO} \approx 3.3$ can be understood by noting that for short run durations the compositions of spinel at the reaction interfaces are closer to the composition in equilibrium with periclase than tothe composition in equilibrium with corundum, this is expected for $D_{Al_2O_3} > D_{MgO}$. In similar experiments Götze and others (2010) determined $D_{MgO} = 1.4 \times 10^{-15} m^2/s$ and $D_{Al_2O_3} = 3.7 \times 10^{-16} m^2/s$ for T = 1350 °C. This is by a factor of about two (D_{MgO}) and 25 ($D_{Al_2O_3}$) slower than the estimates obtained in this study (see table 2). This is ascribed to the fact that in Götze and others (2010) the reaction interfaces were considered as perfectly mobile, and long-range diffusion was considered as the only dissipative process. In our study, the reaction interfaces were considered as having finite mobilities, and part of the free energy decrease associated with spinel growth is dissipated by interface motion. In this case only a fraction of the liberated free energy is available for diffusion. The tracer diffusion coefficients must thus be higher than for the local-equilibrium case to reproduce the experimentally observed growth rate. A self-diffusion coefficient of about $10^{-14} m^2/s$ was determined for diffusion of Al in single crystals of natural spinel at T = 1350 °C by Suzuki and others (2008). This is well in the range of the value determined for a spinel polycrestal in our study. The largely similar Al-diffusivities of a single and a polycrystal probably result from the fact that natural material with trace amounts of Fe and Cr was used in the experiments of Suzuki and others (2008), whereas in the experiments of Jeřabek and others (2014) pure synthetic materials were

[2] Li, C., Griffiths, T., Pennycook, T., Mangler, C., Jeřabek, P., Meyer, J., Habler, G., and R. Abart, R., submitted, The structure of a propagating $MgAl_2O_4$/MgO interface: Linked atomic and μm-scale mechanisms of interface motion: Philosophical Magazine.

used. Moreover, the experiments of Suzuki and others (2008) were done at pressures of 3 to 7 GPa, and are not directly comparable to the 1 bar experiments of Jeřabek and others (2014). The interdiffusion of Fe and Mg in spinel was recently investigated by Vogt and others (2015) in the temperature range of 750 °C to 900 °C. It may be speculated from their results that Fe and Mg diffuse faster than Al, but the data from the latter authors cannot be extrapolated safely to the conditions of our experiments.

Due to finite interface mobilities, the compositions of the newly formed spinel deviate from equilibrium compositions at both reaction interfaces. As a consequence, only a fraction of the theoretically possible free energy change of reaction becomes effective. Accordingly estimates for the kinetic parameters are higher than if spinel grew with its equilibrium compositions and the entire theoretically possible free energy gain were available for driving the kinetic processes such as has been assumed in the study of Götze and others (2014).

The activity for generation/annihilation of vacancies at reaction interfaces was set to $U_{\mathrm{per–sp}} = U_{\mathrm{cor–sp}} \geq 10^{-11}$ to reproduce the experimental observations. This implies that the contribution of non-ideal vacancy formation/annihilation to free energy dissipation is negligible compared to the contributions from long-range diffusion and interface motion.

CONCLUSIONS

Formation of a layer comprised of a solid-solution phase at the contact between two reactant phases of fixed composition by reactive diffusion in a binary system has been investigated. A thermodynamic model has been developed that accounts for several simultaneous dissipative processes including long-range diffusion, migration of the reaction interfaces between the reactant and the product phases as well as generation/annihilation of vacancies at the reaction interfaces. The evolution of the system is governed by the relative rates of these intimately coupled processes. The influence of the respective kinetic parameters on the rate of interlayer growth, on the position of the Kirkendall plane, and on the evolution of the compositions of the solid-solution phase at the reaction interfaces has been investigated. It was found that the compositions of the solid-solution phase at the reaction interfaces are sensitive monitors for deviations from local equilibrium. If the tracer diffusivities of the mobile components are of the same order, finite interface mobility leads to growth of the product phase with compositions that differ from the equilibrium compositions at the reaction interfaces and lie between the solubility limits of the solid-solution phase. If the tracer diffusivities of the mobile components differ significantly the compositions of the solid-solution at the reaction interfaces are displaced from the respective equilibrium values towards higher contents of the less mobile component. This may lead to growth of the solid-solution phase with compositions beyond the solubility limit of the less mobile component. This effect is pronounced, if the mobility of the respective interface and the activity for generation/annihilation of vacancies at the interface are high, and it is suppressed otherwise. Generally, departure from local equilibrium at the reaction interfaces is most pronounced during early growth stages, when interface-reaction control dominates and deviations from parabolic growth occur. With increasing thickness of the layer of the newly formed phase, the system becomes successively more diffusion-controlled, a transition to parabolic growth occurs, and local equilibrium compositions are approached at the reaction interfaces. Interlayer growth experiments in the system $MgO – Al_2O_3$ performed at 1350 °C and atmospheric pressure show that magnesio-aluminate spinel is formed with compositions that are offset from the corresponding equilibrium compositions at both the periclase-spinel and the corundum-spinel interfaces. Application of our thermodynamic model yields estimates for the effective tracer diffusivities, interface mobilities, and activities for generation/annihilation of vacancies at the reaction interfaces.

ACKNOWLEDGMENTS

This project was funded by the DFG project AB 314/2-1 and by the Austrian Science Fund (FWF):I1704-N19 in the framework of the FOR 741 research unit. Help with experimentation by Erik Rybacki and with electron microprobe analyses by Dieter Rhede is gratefully acknowledged. We thank Peter Lichtner, Ralf Dohmen, and Ralf Milke for their constructive reviews.

REFERENCES

Abart, R., and Petrishcheva, E., 2011, Thermodynamic model for reaction rim growth: Interface reaction and diffusion control: American Journal of Science, v. 311, n. 6, p. 517–527, http://dx.doi.org/10.2475/06.2011.02

Abart, R., Kunze, K., Milke, R., Sperb, R., and Heinrich, W., 2004, Silicon and oxygen self-diffusion in enstatite polycrystals: the Milke et al. (2001) rim growth experiments revisited: Contributions to Mineralogy and Petrology, v. 147, n. 6, p. 633–646, http://dx.doi.org/10.1007/s00410-004-0596-9

Abart, R., Petrishcheva, E., Fischer, F. D., and Svoboda, J., 2009, Thermodynamic model for diffusion controlled reaction rim growth in a binary system: Application to the forsterite-enstatite-quartz system: American Journal of Science, v. 309, n. 2, p. 114–131, http://dx.doi.org/10.2475/02.2009.02

Andreozzi, G., and Princivalle, F., 2002, Kinetics of cation ordering in synthetic $MgAl_2O_4$ spinel: American Mineralogist, v. 87, n. 7, p. 838–844, http://dx.doi.org/10.2138/am-2002-0705

Andreozzi, G. B., Princivalle, F., Skogby, H., and della Giusta, A., 2000, Cation ordering and structural variations with temperature in $MgAl_2O_4$ spinel: An x-ray single-crystal study: American Mineralogist, v. 85, n. 9, p. 1164–1171, http://dx.doi.org/10.2138/am-2000-8-907

Balluffi, R., Allen, S., and Carter, W., 2005, Kinetics of Materials: Hoboken, New Jersey, John Wiley & Sons Inc., 627 p.

Brady, J., 1983, Intergranular diffusion in metamorphic rocks: American Journal of Science, v. 283-A, p. 181–200.

Callen, H. B., 1985, Thermodynamics and an introduction to thermostatistics: Hoboken, New Jersey, John Wiley and Sons, 2 edition, 493 p.

Carter, R., 1961, Mechanism of solid-state reaction between magnesium oxide and aluminum oxide and between magnesium oxide and ferric oxide: Journal of the American Ceramic Society, v. 44, n. 3, p. 116–120, http://dx.doi.org/10.1111/j.1151-2916.1961.tb13724.x

Cserháti, C., Balogh, Z., Csik, A., Langer, G. A., Erdelyi, Z., Glodán, Gy., Katona, G. L., Beke, D. L, Zizak, I., Darowski, N., Dudzik, E., and Feyerherm, R., 2008, Linear growth kinetics of nanometric silicides in co/amorphous-Si and co/coSi/amorphous-Si thin films: Journal of Applied Physics, v. 104, 024311, http://dx.doi.org/10.1063/1.2957071

De Groot, S. R., and Mazur, P., 1984, Non-Equilibrium Thermodynamics: New York, Dover Publications, 510 p.

Deal, B. E., and Grove, A. S., 1965, General relationship for thermal oxidation of silicon: Journal of Applied Physics, v. 36, p. 3770–3778, http://dx.doi.org/10.1063/1.1713945

Dybkov, V. I., 1986, Reaction diffusion in heterogeneous binary systems. Part 2 Growth of the chemical compound layers at the interface between two elementary substances: two compound layers: Journal of Materials Science, v. 21, n. 9, p. 3085–3090, http://dx.doi.org/10.1007/BF00553340

Farrell, H. H., Gilmer, G. H., and Suenaga, M., 1975, Diffusion mechanisms for growth of Nb_3Sn intermetallic layers: Thin Solid Films, v. 25, n. 1, p. 253–264, http://dx.doi.org/10.1016/0040-6090(75)90261-8

Fischer, F. D., Svoboda, J., and Petryk, H., 2014, Thermodynamic extremal principles for irreversible processes in materials science: Acta Materialia, v. 67, p. 1–20, http://dx.doi.org/10.1016/j.actamat.2013.11.050

Fisler, D. K., Mackwell, S. J., and Petsch, S., 1997, Grain boundary diffusion in enstatite: Physics and Chemistry of Minerals, v. 24, n. 4, p. 264–273, http://dx.doi.org/10.1007/s002690050038

Gamsjäger, E., 2007, A note on the contact conditions at migrating interfaces: Acta Materialia, v. 55, n. 14, p. 4823–4833, http://dx.doi.org/10.1016/j.actamat.2007.04.050

Gardes, E., Wunder, B., Wirth, R., and Heinrich, W., 2011, Growth of multilayered polycrystalline reaction rims in the MgO-SiO_2 system, part I: experiments. Contributions to Mineralogy Petrology, v. 161, n. 1, p. 1–12, http://dx.doi.org/10.1007/s00410-010-0517-z

Gobbi, G. C., Christoffersen, R., Otten, M. T., Miner, B., Buseck, P. R., Kennedy, G. J., and Fyfe, C. A., 1985, Direct determination of cation disorder in $MgAl_2O_4$ spinel by high resolution ^{27}Al magic-angle-spinning nmr spectroscopy: Chemical Letters, v. 14, n. 6, p. 771–774, http://dx.doi.org/10.1246/cl.1985.771

Gösele, R., and Tu, K. N., 1982, Growth kinetics of planar binary diffusion couples: "Thin- film case" versus "bulk cases": Journal of Applied Physics, v. 53, p. 3252–3260, http://dx.doi.org/10.1063/1.331028

Götze, L. C., Abart, R., Rybacki, E., Keller, L. M., Petrishcheva, E., and Dresen, G., 2010, Reaction rim growth in the system $MgAl_2O_3$-SiO_2 under uniaxial stress: Mineralogy and Petrology, v. 99, n. 3, p. 263–277, http://dx.doi.org/10.1007/s00710-009-0080-3

Götze, L. C., Abart, R., Milke, R., Schorr, S., Zizak, I., Dohmen, R., and Wirth, R., 2014, Growth of magnesio-aluminate spinel in thin film geometry - *in-situ* monitoring using synchrotron x-ray diffraction and thermodynamic model: Physics and Chemistry of Minerals, v. 44, n. 9, p. 681–693, http://dx.doi.org/10.1007/s00269-014-0682-0

Hallstedt, B., 1992, Thermodynamic assessment of the system $MgAl_2O_3$: Journal of the American Ceramic Society, v. 75, n. 6, p. 1497–1507, http://dx.doi.org/10.1111/j.1151-2916.1992.tb04216.x

Hesse, D., Senz, ST., Scholz, R., Werner, P., and Heydenreich, J., 1994, Structure and morphology of the reaction fronts during the formation of $MgAl_2O_4$ thin films by solid state reaction between *R*-cut sapphire substrates and MgO films: Interface Science, v. 2, n. 3, p. 221–237, http://dx.doi.org/10.1007/BF00215169

Jeřabek, P., Abart, R., Rybacki, E., and Habler, G., 2014, Microstructure and texture evolution during growth of magnesio-aluminate spinel at corundum – periclase interfaces under uniaxial load: The effect of stress concentration on reaction progress: American Journal of Science, v. 314, n. 5, p. 1–26, http://dx.doi.org/10.2475/05.2014.02

Jung, I-H., Decterov, S. A., and Pelton, A. D., 2004, Critical thermodynamic evaluation and optimization of the MgO-Al_2O_3, CaO-MgO- Al_2O_3, and MgO-Al_2O_3-SiO_2 systems: Journal of Phase Equilibria and Diffusion, v. 25, n. 4, p. 329–345, http://dx.doi.org/10.1007/s11669-004-0151-4

Keller, L. M., Götze, L. C., Rybacki, E., Dresen, G., and Abart, R., 2010, Enhancement of solid-state reaction rates by non-hydrostatic stress effects on polycrystalline diffusion kinetics: American Mineralogist, v. 95, n. 10, p. 1399–1407, http://dx.doi.org/10.2138/am.2010.3372

Koch, E., and Wagner, C., 1936, Formation of Ag_2HgI_4 from AgI and HgI_2 by reaction in the solid state: Zeitschrift für Physikalische Chemie, v. 34, p. 317–321,

Liu, C-M., Chen, J-C., and Chen, C-J., 2005, The growth of an epitaxial Mg-Al spinel layer on sapphire by solid-state reactions: Journal of Crystal Growth, v. 285, n. 1–2, p. 275–283, http://dx.doi.org/10.1016/j.jcrysgro.2005.08.023

Martyushev, L. M., and Seleznev, V. D., 2006, Maximum entropy production principle in physics, chemistry and biology: Physics Reports, v. 426, n. 1, p. 1–45, http://dx.doi.org/10.1016/j.physrep.2005.12.001

Milke, R., and Heinrich, W., 2002, Diffusion-controlled growth of wollastonite rims between quartz and calcite: Comparison between nature and experiment: Journal of Metamorphic Geology, v. 20, n. 5, p. 467–480, http://dx.doi.org/10.1046/j.1525-1314.2002.00384.x

Milke, R., Wiedenbeck, M., and Heinrich, W., 2001, Grain boundary diffusion of Si, Mg, and O in enstatite reaction rims: a sims study using isotopically doped reactants: Contributions to Mineralogy and Petrology, v. 142, n. 1, p. 15–26, http://dx.doi.org/10.1007/s004100100277

Millard, R. L., Peterson, R. C., and Hunter, B. K., 1992, Temperature dependence of cation disorder in $MgAl_2O_4$ spinel using ^{27}Al and ^{17}O magic angle spinning nmr: American Mineralogist, v. 77, n. 1–2, p. 44–52.

Navias, L., 1961, Preparation and properties of spinel made by vapor transport and diffusion in the system $MgAl_2O_3$: Journal of the American Ceramic Society, v. 44, n. 9, p. 434–446, http://dx.doi.org/10.1111/j.1151-2916.1961.tb13752.x

Onsager, L., 1931, Reciprocal relations in irreversible processes. I: Physical Review, v. 37, n. 4, p. 405–426, http://dx.doi.org/10.1103/PhysRev.37.405

Pavese, A., Artioli, G., and Hoser, A., 2000, $MgAl_2O_4$ synthetic spinel: cation and vacancy distribution as a function of temperature, from *in situ* neutron powder diffraction: Zeitschrift für Kristallographie, v. 21, p. 406–412,

Pfeiffer, T., and Schmalzried, H., 1989, Spinel formation: A detailed analysis: Zeitschrift für Physikalische Chemie, v. 161, p. 1–17, http://dx.doi.org/10.1524/zpch.1989.161.Part_1_2.001

Rossi, R., and Fulrath, R., 1963, Epitaxial growth of spinel by reaction in the solid state: Journal of the American Ceramic Society, v. 46, n. 3, p. 145–149, http://dx.doi.org/10.1111/j.1151-2916.1963.tb11699.x

Sack, R. O., 1982, Spinels as petrogenetic indicators: Activity-composition relations at low pressures: Contributions to Mineralogy and Petrology, v. 79, n. 2, p. 169–186, http://dx.doi.org/10.1007/BF01132886

——— 2014, $MgAl_2O_4$–$Al_{8/3}O_4$ spinels: Formulation and calibration of the low pressure thermodynamics of mixing: American Journal of Science, v. 314, n. 4, p. 858–877, http://dx.doi.org/10.2475/04.2014.02

Sack, R. O., and Ghiorso, M. S., 1991, An internally consistent model for the thermodynamic properties of Fe- Mg-titanomagnetite-a|uminate spinels: Contributions to Mineralogy and Petrology, v. 106, n. 4, p. 474–505, http://dx.doi.org/10.1007/BF00321989

Schmalzried, H., 1962, Reaktionsmechanism der spinellbildung im festen zustand: Zeitschrift für Physikalische Chemie, v. 33, n. 1–4, p. 111–128, http://dx.doi.org/10.1524/zpch.1962.33.1_4.111

——— 1974, Solid-state reactions between oxides, *in* Seltzer, M., and Jaffee, R., editors, Defects and transport in oxides: New York, Plenum Press, p. 83–108.

——— 1981, Solid State Reactions: Weinheim, Germany, Verlag Chemie, p. 107.

Schneider, A., and Inden G., 2004, Computer simulation of diffusion controlled phase transformations, *in* Raabe, D., Roters, F., Barlat, F., and Chen, L., editors, Continuum Scale Simulation of Engineering Materials-Fundamentals-Microstructures-Process Applications: Weinheim, GermanyWiley-VCH, p. 3–36, http://dx.doi.org/10.1002/3527603786.ch1

Sieber, H., Hesse, D., and Werner, P., 1997a, Misfit accommodation mechanisms at moving reaction fronts during topotaxial spinel-forming thin-film solid-state reactions: A high-resolution transmission electron microscopy study of five spinels of different misfits: Philosophical Magazine A, v. 75, n. 4, p. 889–908, http://dx.doi.org/10.1080/01418619708214000

Sieber, H., Werner, P., and Hesse, D., 1997b, The atomic structure of the reaction front as a function of the kinetic regime of a spinel-forming solid-state reaction: Philosophical Magazine A, v. 75, n. 4, p. 909–924, http://dx.doi.org/10.1080/01418619708214001

Suzuki, A. M., Yasuda, A., and Ozawa, K., 2008, Cr and al diffusion in chromite spinel: Experimental determination and its implication for diffusion creep: Physics and Chemistry of Minerals, v. 35, p. 433–445, http://dx.doi.org/10.1007/s00269-008-0238-2

Svoboda, J., and Fischer, F. D., 2013, A new computational treatment of reactive diffusion in binary systems: Computational Materials Science, v. 78, p. 39–46, http://dx.doi.org/10.1016/j.commatsci.2013.05.012
Svoboda, J., and Turek, I., 1991, On diffusion-controlled evolution of closed solid-state thermodynamic systems at constant temperature and pressure: Philosophical Magazine, Part B, v. 64, n. 6, p. 749–759, http://dx.doi.org/10.1080/13642819108207635
Svoboda, J., Turek, I., and Fischer, F. D., 2005, Application of the thermodynamic extremal principle to modeling of thermodynamic processes in material sciences: Philosophical Magazine, v. 85, n. 31, p. 3699–3707, http://dx.doi.org/10.1080/14786430500267760
Svoboda, J., Gasmjaeger, E., Fischer, F. D., and Kozeschnik, E., 2006, Modeling of kinetics of diffusive phase transformation in binary systems with multiple stoichiometric phases: Journal of Phase Equilibria and Diffusion, v. 27, n. 6, p. 622–628, http://dx.doi.org/10.1007/BF02736564
van Dal, M. J. H., Pleumeerkers, M. C. L. P., Kondentsov, A. A., and van Loo, F. J. J., 2000a, Diffusion studies and re-examination of the Kirkendall effect in the Au-Ni system: Journal of Alloys and Compounds, v. 309, n. 1–2, p. 132–140, http://dx.doi.org/10.1016/S0925-8388(00)01056-2
——— 2000b, Intrinsic diffusion and Kirkendall effect in Ni-Pd and Fe-Pd solid solutions: Acta Materialia, v. 48, n. 2, p. 385–396, http://dx.doi.org/10.1016/S1359-6454(99)00375-4
Vernon, R. H., 2004, A practical guide to rock microstructure: Cambridge, England, University Press, 606 p.
Vogt, K., Dohmen, R., and Chakraborty, S., 2015, Fe-Mg diffusion in spinel: New experimental data and a point defect model: American Mineralogist, v. 100, n. 10, p. 2112–2122, http://dx.doi.org/10.2138/am-2015-5109
Watson, E. B., and Price, J. D., 2002, Kinetics of the reaction MgO + Al_2O_3 → $3MgAl_2O_4$ and Al-Mg interdiffusion in spinel at 1200 to 2000 °C and 1.0 to 4.0 Gpa: Geochimica et Cosmochimica Acta, v. 66, n. 12, p. 2123–2138, http://dx.doi.org/10.1016/S0016-7037(02)00827-X
Whitney, W., II, and Stubican, V. S., 1971, Interdiffusion studies in the system MgO – Al_2O_3; Journal of Physics and Chemistry of Solids, v. 32, n. 2, p. 305–312, http://dx.doi.org/10.1016/0022-3697(71)90015-1
Wood, B. J., Kirkpatrick, R. J., and Montez, B. A., 1986, Order-disorder phenomena in $MgAl_2O_4$ spinel: American Mineralogist, v. 71, n. 7–8, p. 999–1006.
Yund, R. A., 1997, Rates of grain boundary diffusion through enstatite and forsterite reaction rims: Contributions to Mineralogy and Petrology, v. 126, n. 3, p. 224–236, http://dx.doi.org/10.1007/s004100050246
Zhang, P., DebRoy, T., and Seetharaman, S., 1996, Interdiffusion in the $MgAl_2O_4$ spinel with or without some dopants: Metallurgical and Materials Transactions A, v. 27, n. 8, p. 2105–2114, http://dx.doi.org/10.1007/BF02651865
Ziegler, H., 1961, Two extremal principles in irreversible thermodynamics: Ingenieur- Archiv, v. 30, n. 6, p. 410–416, http://dx.doi.org/10.1007/BF00531783
Zienert, T., and Fabrichnaya, O., 2013, Thermodynamic assessment and experiments in the system MgO-Al_2O3: CALPHAD, v. 40, p. 1–9, http://dx.doi.org/10.1016/j.calphad.2012.10.001